Cavendish–HEP–96/2
hep-ph/9607441

DEEP INELASTIC SCATTERING — THEORY AND PHENOMENOLOGY [a]

B.R. WEBBER
Cavendish Laboratory, University of Cambridge,
Madingley Road, Cambridge CB3 0HE, England

Recent developments in theory and phenomenology relevant to deep inelastic lepton scattering are reviewed, concentrating on the following topics: predicted behaviour of non-singlet and polarized structure functions at small x; theoretical studies of saturation and unitarity effects at small x in quarkonium scattering; renormalons and higher twist contributions; next-to-leading-order calculations of jet cross sections; forward jet production as a probe of small-x dynamics.

1 Introduction

The aim of this introductory review is to highlight some theoretical and phenomenological work done in the past year or so which may be relevant to deep inelastic scattering (DIS). The selection of topics is of course subjective; it is intended to cover a range of physics somewhat superficially, relying on the talks to be presented in the working groups to fill in the details.

In the important field of small-x physics, I have chosen to concentrate on rather non-standard topics: the small-x behaviour of non-singlet and polarized structure functions, and the small-x dynamics of (quark)onium. This is because there has been interesting new work in these areas, whereas in the main arena of unpolarized singlet structure we are experiencing something of a lull until more precise calculations become available.

On the large topic of diffractive DIS I also have little to say, although the study of multi-pomeron exchange in onium scattering is relevant. The main developments in this area are experimental at present and substantial theoretical progress may be expected to come later.

I have included a rather speculative section on renormalons, because this is a fashionable topic throughout QCD at present, and it might just give some indication of where progress could be made on the difficult problem of higher-twist contributions.

[a] Talk at DIS96, International Workshop on Deep Inelastic Scattering and Related Phenomena, Rome, April 1996.

Finally I discuss jet production, for which important new calculations have been completed, although the situation on their comparison with older calculations and with experiment is still unclear.

2 Non-Singlet and Polarized Structure Functions at Small x

There is a lot of interesting physics associated with the behaviour of non-singlet and polarized structure functions, for example that connected with sum rules. The Gottfried sum

$$\int_0^1 \frac{dx}{x}(F_2^p - F_2^n) \simeq \tfrac{1}{3}\left[1 + \int_0^1 dx(\bar{u} - \bar{d})\right] \tag{1}$$

reveals that the $\bar{u}$ and $\bar{d}$ distributions are not the same, while the Gross–Llewellyn-Smith and Bjorken sum rules

$$\begin{aligned} \int_0^1 dx(F_3^\nu + F_3^{\bar{\nu}}) &= 6\left[1 - \frac{\alpha_s}{\pi} - 3.6\left(\frac{\alpha_s}{\pi}\right)^2 - 19\left(\frac{\alpha_s}{\pi}\right)^3 + \ldots\right], & (2) \\ \int_0^1 dx(g_1^p - g_1^n) &= \frac{1}{6}\left|\frac{g_A}{g_V}\right|\left[1 - \frac{\alpha_s}{\pi} - 3.6\left(\frac{\alpha_s}{\pi}\right)^2 - 20\left(\frac{\alpha_s}{\pi}\right)^3 + \ldots\right] & (3) \end{aligned}$$

provide precise determinations [1,2] of α_s. The Ellis-Jaffe sum rule for g_1^p alone suggested the "proton spin crisis". All these sum rules require assumptions about how to extrapolate non-singlet quantities towards $x = 0$, so we need to understand just what QCD predicts on this point. This is an area where there has been recent progress in theory and phenomenology.

First let us recall what happens in the unpolarized, singlet case. The behaviour is dominated by ladder graphs with longitudinally polarized gluons on each side, Fig. 1(a), which give a basic x^{-1} dependence to the gluon distribution $g(x)$ and hence to the structure functions. In DGLAP (leading-log Q^2) evolution,[3] this is modified by a relatively slowly-varying asymptotic factor,

$$g(x) \sim \frac{1}{x}\exp\left(\sqrt{4C_A\frac{\alpha_s}{\pi}\ln\frac{Q^2}{Q_0^2}\ln\frac{1}{x}}\right) \qquad \text{(DGLAP)}. \tag{4}$$

The presence of two large logarithms for each power of α_s is characteristic. Here one keeps only those terms in which one of them is a $\log Q^2$. These come from the region of phase space in which the transverse momenta k_T of the exchanged gluons are ordered along the ladder.

At small x we need to keep instead the terms with the largest number of factors of $\log x$. The k_T-ordering breaks down, and there is the possibility of

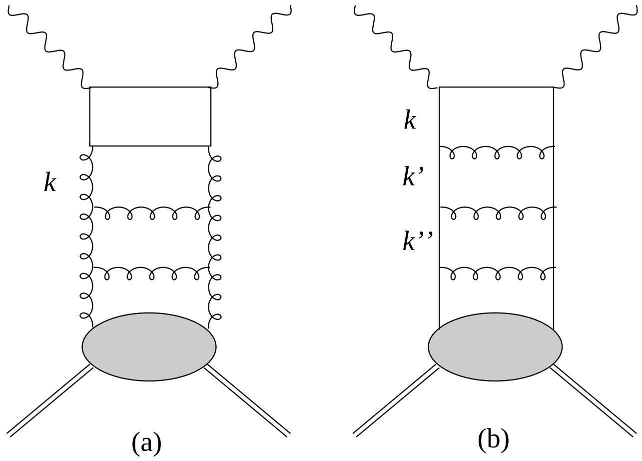

Figure 1: (a) Gluon ladder and (b) quark ladder graphs, contributing to singlet and non-singlet structure functions respectively.

double-logarithmic $(\alpha_s \ln^2 x)^n$ terms. However, BFKL [4] showed that double logs of x cancel in the fully inclusive, unpolarized, singlet structure functions. Although k_T is not ordered, it diffuses without violent fluctuations. This leads to the asymptotic behaviour

$$g(x) \sim \frac{1}{x} \exp\left(\chi_S C_A \frac{\alpha_s}{\pi} \ln\frac{1}{x}\right) \sim x^{-1-\gamma_S} \qquad \text{(BFKL)}. \tag{5}$$

The leading singlet BFKL eigenvalue $\chi_S = 4\ln 2$ implies that $\gamma_S \simeq 0.5$ for $\alpha_s \simeq 0.2$.

The observed behaviour is consistent with next-to-leading-order (NLO) DGLAP evolution, and with the leading-order BFKL form (5) for a reduced value of γ_S. It is expected that non-leading corrections to the BFKL prediction will be important. They are not yet known, but progress is being made on calculating them.[5]

2.1 Non-Singlet Structure Functions at Small x

For a non-singlet quantity $f(x)$, such as $(F_2^p - F_2^n)/x$, we have quarks instead of gluons at the sides of the ladder, as in Fig. 1(b), and leading log-Q^2 evolution now gives

$$f(x) \sim \frac{1}{x^0} \exp\left(\sqrt{2C_F \frac{\alpha_s}{\pi} \ln\frac{Q^2}{Q_0^2} \ln\frac{1}{x}}\right) \qquad \text{(DGLAP)}. \tag{6}$$

However, in this case the leading log-x terms are double-logarithmic.[6,7] Using a Sudakov representation of the exchanged momenta,

$$k^\mu = xp^\mu + y\tilde{q}^\mu + k_T^\mu\;, \tag{7}$$

where $\tilde{q} = q + xp$ (so that $\tilde{q}^2 = 0$), the double logarithms come from the region in which both momentum fractions are strongly ordered, but in opposite directions:

$$x \ll x' \ll x'' \ll \cdots\;, \quad y \gg y' \gg y'' \gg \cdots\;. \tag{8}$$

The dominant region of transverse momenta now becomes

$$k_T^2/x > {k'}_T^2/x' > {k''}_T^2/x'' > \cdots\;. \tag{9}$$

Thus there can be huge fluctuations along the ladder, and the breakdown of k_T ordering is much more drastic than in the singlet case. This leads to the Kirschner-Lipatov [6] (KL) type of small-x behaviour:

$$f(x) \sim \frac{1}{x^0} \exp\left(\sqrt{2C_F \frac{\alpha_s}{\pi} \ln^2\frac{1}{x}}\right) \sim x^{-\gamma_{NS}^{(+)}} \qquad \text{(KL)} \tag{10}$$

where $\gamma_{NS}^{(+)} = \sqrt{2C_F\alpha_s/\pi} \simeq 0.4$ for $\alpha_s \simeq 0.2$. Note that Regge behaviour [8] at small x would imply that

$$f(x) \sim x^{-\alpha_\rho} \quad \text{with } \alpha_\rho \simeq \tfrac{1}{2} \qquad \text{(R)}, \tag{11}$$

which is similar.

2.2 Polarized Structure Functions at Small x

The structure function combination $\Delta g_1 = g_1^p - g_1^n$ appearing in the Bjorken sum rule depends on the odd-signature part of the forward virtual Compton amplitude (i.e. odd under s-u crossing). Therefore the expected Regge behaviour is that associated with exchange of the odd-signature, isovector a_1 trajectory,

$$\Delta g_1(x) \sim x^{-\alpha_{a_1}} \quad \text{with } \alpha_{a_1} \simeq 0 \qquad \text{(R)}. \tag{12}$$

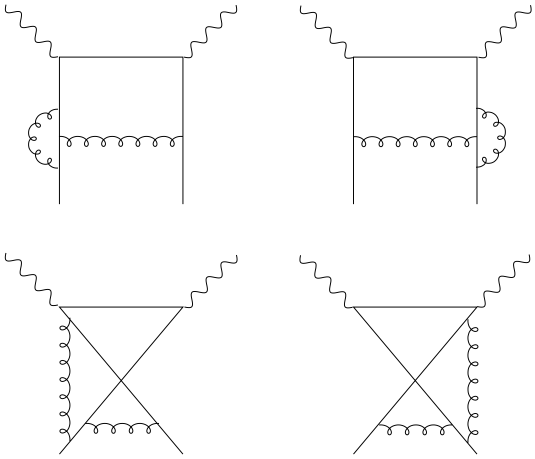

Figure 2: Non-ladder contributions that cancel for even-signature structure functions but not for odd signature.

Using the KL approach,[6] however, Bartels, Ermolaev and Ryskin [9] (BER) find that the corresponding power $\gamma_{NS}^{(-)}$ is actually slightly *larger* than that for even signature:

$$\Delta g_1(x) \sim x^{-\gamma_{NS}^{(-)}} > x^{-\gamma_{NS}^{(+)}} \sim x^{-0.4} \qquad \text{(BER)}, \tag{13}$$

and so the behaviour as $x \to 0$ is more singular.

The reason for the difference between even and odd signature is that there are non-ladder contributions, like those in Fig. 2, which cancel in the former case but not in the latter. The even-signature cancellation follows from the fact that the system exchanged in the t-channel is a colour singlet. The surprising thing is that the non-ladder terms enhance the odd-signature contribution rather than reducing it.

An investigation of the phenomenological consequences for Δg_1 has been presented recently.[10] Fig. 3 shows the results of resumming the large logarithms of x as discussed above, compared with those of the standard next-to-leading order DGLAP evolution. A difficulty with the resummation is that the leading log-x expressions do not conserve fermion number, i.e. the integrals of the resummed splitting functions do not vanish. One can fix this in various *ad hoc* ways which do not affect the small-x behaviour. The most extreme (curve A in Fig. 3) is to add a δ-function contribution at $x = 1$. Curve B represents a less drastic prescription.[10] We see that the effect in either case is not great at foreseeable values of x and Q^2.

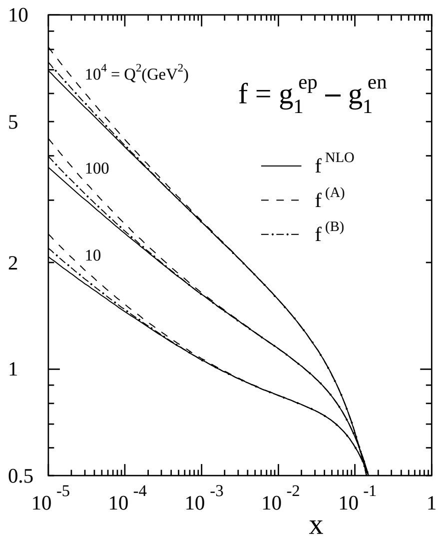

Figure 3: Small-x evolution of $g_1^p - g_1^n$. A and B denote different prescriptions for fermion number conservation (see text).

The singlet contribution to g_1 at small x has also been considered.[11] Here gluon ladders like Fig. 1(a) can contribute, but only one of the gluons on the sides can be longitudinal, and so the basic power behaviour is $x^{-1+1} = x^0$, the same as for quark ladders, Fig. 1(b). Again, the odd signature of g_1 means that non-ladder contributions like those in Fig. 2 do not cancel and in fact enhance the structure function. The asymptotic form is

$$g_1(x) \sim \exp\left(\zeta_S \sqrt{C_A \frac{\alpha_s}{\pi} \ln^2 \frac{1}{x}}\right) \sim x^{-\gamma_S^{(-)}} \qquad \text{(BER)}. \tag{14}$$

The gluonic contribution alone would give $\zeta_S = 4$ and hence $\gamma_S^{(-)} = 3\gamma_{NS}^{(-)} \simeq 1.2$. Mixing with quark exchange reduces the leading eigenvalue slightly:

$$\zeta_S \simeq 3.5\;, \quad \gamma_S^{(-)} \simeq 1.0\;, \tag{15}$$

implying that $g_1(x) \sim x^{-1}$. Further experimental data on the small-x behaviour of g_1 are needed to test this surprising prediction. The theoretical analysis[11] suggests other remarkable features, such as a possible change in the sign of the polarized gluon distribution between large and small x.

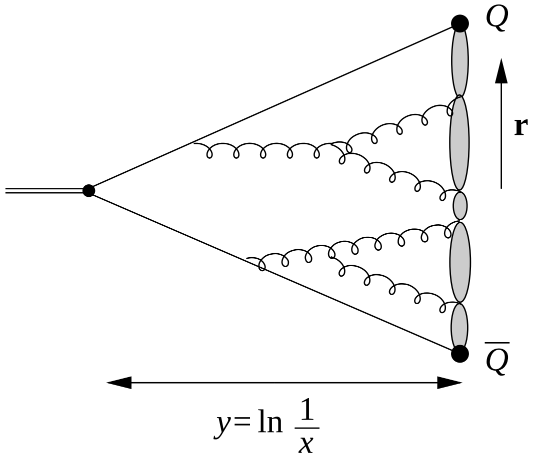

Figure 4: Development of dipole chain in onium wave function.

3 Small-x Saturation and Unitarity in Onium–Onium Scattering

Amongst the important new phenomena expected in deep inelastic scattering at small x are parton saturation and unitarity corrections.[12] As the parton density increases, interactions between partons become more significant and limit the rate of growth of the density (saturation). In addition, multiple scattering effects become necessary in order to prevent cross sections from exceeding unitarity limits. These phenomena are difficult to predict reliably in the case of ep scattering because the proton is a large object whose structure cannot be computed perturbatively. To study them within the domain of perturbation theory we need to consider a smaller system such as a heavy quark-antiquark bound state. For a sufficiently large quark mass m_Q, the size of such a state is $R \sim 1/\alpha_s m_Q$. Then the strong coupling at the relevant momentum scale $q^2 \sim 1/R^2$ will be small enough for a perturbative expansion in $\alpha_s(q^2)$ to be applicable.

The theory of low-x phenomena in quarkonium (often simply called onium) has been worked out in some detail over the last couple of years using the colour dipole formulation[13–20] of QCD at small x. The dipole formulation is based on the fact that, to leading order in the number of colours, the light-cone wave function of an onium state can be represented by a chain of colour dipoles linking the heavy quark and antiquark (Fig. 4). As the wave function is probed at smaller x, i.e. higher 'rapidity' $y = \ln(1/x)$, more and more dipoles are likely to be resolved. The evolution of the dipole configurations with increasing y can be formulated as a branching process governed by the BFKL evolution equation. It turns out to be most convenient to describe the wave function in a (transverse position, rapidity) ($\mathbf{r}$,y) representation. The mean density of dipoles of size c at a distance r from a primary onium ($Q\bar{Q}$) dipole of size b is found to be

$$\bar{n}(b,c,r,y) \sim \exp\left[(\alpha_P - 1)y - \frac{\ln^2(16r^2/bc)}{ky}\right] \tag{16}$$

where

$$\alpha_P = 1 + 4\ln 2\, C_A\alpha_s/\pi \tag{17}$$

is the BFKL pomeron intercept and

$$k = 14\zeta(3)\, C_A\alpha_s/\pi \tag{18}$$

is the corresponding diffusion constant. Thus as y increases the dipole density grows in the expected manner and dipoles diffuse slowly (logarithmically in $\mathbf{r}$) from the onium source. The growth of dipole density leads to saturation and unitarity effects that can be investigated using the 'theoretical laboratory' of onium physics.[b]

3.1 Onium–Onium Scattering

To study the effects of unitarity it is simplest to consider onium-onium elastic scattering [13–17] at very high energy $\sqrt{s}$. The onia pass through each other with relative rapidity $Y \sim \ln(s/m_Q^2)$ at some relative impact parameter $\mathbf{r}$. In the centre-of-mass frame, the dominant elastic process is two-gluon exchange between dipoles in the two onium wave functions evolved to rapidity $y = Y/2$. This corresponds to exchange of a single BFKL pomeron: the two evolved wave functions provide the upper and lower halves of a gluon ladder, which are joined in the middle by the two exchanged gluons. The two-gluon exchange interaction is short-ranged (it falls off like $1/r^4$ at large transverse distances), and so only those dipole that overlap contribute significantly to the scattering amplitude.

Fig. 5 illustrates the situation for the two typical onium configurations shown at the top.[c] The impact parameter profile of the one-pomeron amplitude, shown lower left, is obtained by moving one configuration over the other

---

[b]Applications of the dipole formulation to DIS phenomenology are also being investigated.[18–20]

[c]This figure and the results that follow were obtained by Salam [16] using his Monte Carlo program OEDIPUS [21] (Onium Evolution, Dipole Interaction, Perturbative Unitarization Software).

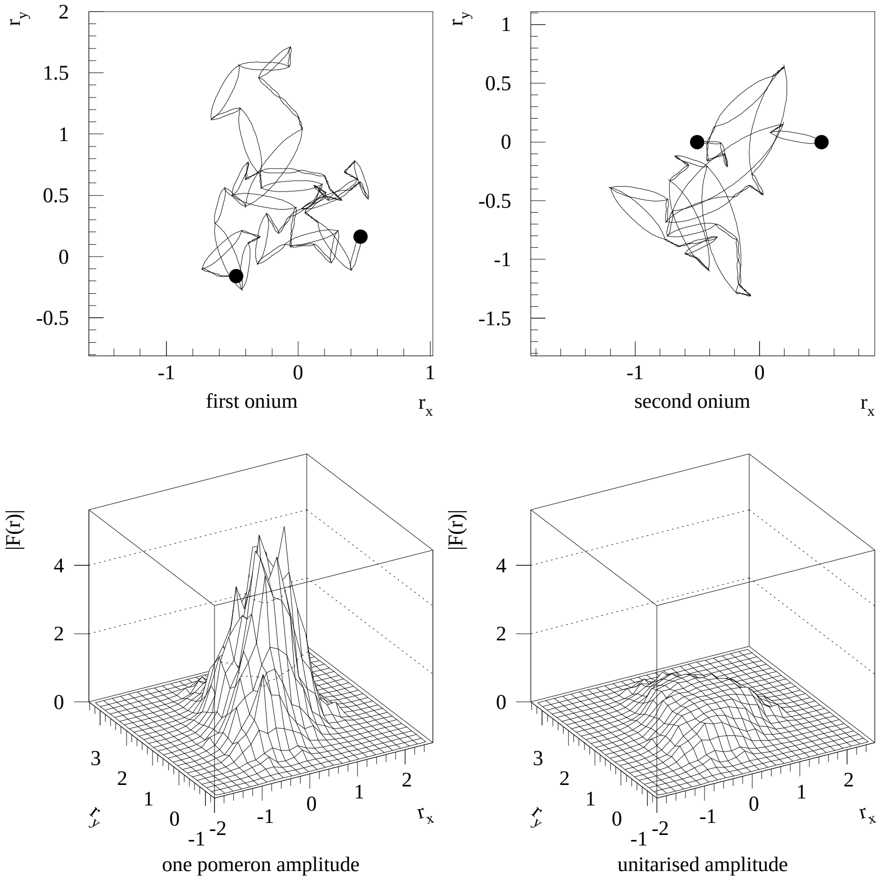

Figure 5: Typical onium dipole configurations and their one-pomeron and unitarized interaction amplitudes.

and computing the sum of the two-gluon exchange amplitudes between all pairs of dipoles at each relative position. Thus at impact parameters for which many dipoles overlap the one-pomeron amplitude violates the unitarity limit, as shown by the spikes exceeding unity.

3.2 Unitarity and Saturation

Schematically, the elastic S-matrix element for single pomeron exchange has the form

$$S = 1 - \sum_{\gamma,\gamma'} P_\gamma P_{\gamma'} f_{\gamma,\gamma'} \tag{19}$$

where γ and γ' represent dipole configurations of the two onia with probabilities P_γ and $P_{\gamma'}$ respectively, and $if_{\gamma,\gamma'}$ is the one-pomeron amplitude for those configurations. To satisfy unitarity we need to take into account multiple pomeron exchange. For large dipole multiplicities the n-pomeron amplitude exponentiates, i.e.

$$S = 1 - \sum_n \sum_{\gamma,\gamma'} P_\gamma P_{\gamma'} f^{(n)}_{\gamma,\gamma'} \tag{20}$$

where

$$f^{(n)}_{\gamma,\gamma'} \sim -\frac{(-f_{\gamma,\gamma'})^n}{n!} \tag{21}$$

and hence

$$S \sim \sum_{\gamma,\gamma'} P_\gamma P_{\gamma'} \exp(-f_{\gamma,\gamma'}) \ . \tag{22}$$

This ensures that the elastic amplitude never exceeds the unitarity limit, as illustrated for the particular configurations in Fig. 5 by the profile on the lower right. The resulting changes in the total and elastic cross sections as functions of rapidity are shown in Fig. 6.

We see that the one-pomeron total and elastic cross sections have the expected energy dependences, s^{α_P-1} and $s^{2(\alpha_P-1)}$ respectively. The unitarized total cross section has a somewhat reduced effective power, while the elastic is more strongly affected. This is because elastic scattering is more dominated by smaller impact parameters, where large dipole densities are more probable.

When one performs the sum over multiple pomeron exchanges first, and then the sum over dipole configurations, as in Eq. (22), it is obvious that a stable, unitary result is obtained. On the other hand one may evaluate the terms in Eq. (20) separately for each n, by summing over configurations first. However, the multiple scattering series so obtained is strongly divergent.[13,16] The reason is that the configuration probability distributions P_γ and $P_{\gamma'}$ have

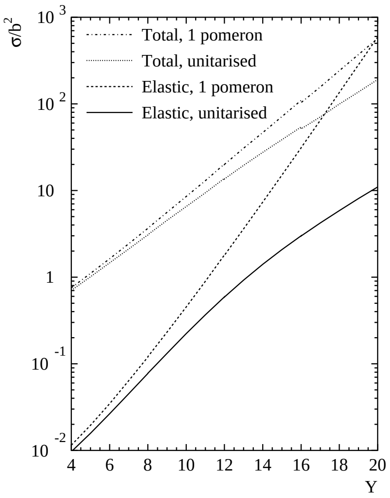

Figure 6: Onium-onium total and elastic scattering cross sections.

long (exponential) tails at high dipole multiplicities, which become dominant at high n but are strongly suppressed after summation over n. This suggests that for light hadrons also an expansion in terms of the number of pomerons exchanged may not be useful at very high energies.

So far, we have discussed everything in the onium-onium centre-of-mass frame, where the two onia evolve through equal rapidity intervals, $y = Y/2$. We could equally well consider a 'fixed-target' type of frame, in which one onium evolves through $y \sim Y$ and the other remains close to a pure $Q\bar{Q}$ configuration. One can show that the above treatment is frame-independent at the level of one-pomeron (two-gluon) exchange, but the results for multiple exchange are frame dependent. The reason is that multiple scattering in the c.m. frame looks like parton-parton interaction (saturation) in the wave function of the moving onium as seen from the rest frame of the other. Thus unitarity and saturation effects are intimately related, and one can learn about saturation by enforcing the condition that the simultaneous treatment of the two phenomena should be frame-independent.[17] The reader is referred to the talk by Salam[22] for further details.

4 Renormalons and Higher Twist

An important thing to bear in mind when computing predictions of perturbative QCD is that the perturbation series is not expected to converge. There may already be indications of this in some quantities relevant to DIS: for example, the perturbative coefficients in the Gross–Llewellyn-Smith and Bjorken sum rules, Eqs. (2) and (3), are growing rapidly.

A known source of divergence of the perturbative expansion is the set of so-called *renormalon* graphs,[23] illustrated in Fig. 7. Summing chains of vacuum polarization bubbles on the gluon line leads to a prediction of the form

$$F = \sum_n c_n \alpha_s^n \tag{23}$$

where the coefficients c_n are factorially divergent at high orders:

$$c_n \sim n!\,(b/p)^n \ , \tag{24}$$

p being a rational number that depends on the particular quantity F being evaluated. Including n_f flavours of fermionic bubbles like those shown in Fig. 7, one finds $b = -n_f/6\pi$. To take account of gluonic bubbles as well, the 'naive non-Abelianization' procedure [24–30] is generally adopted: one evaluates the graphs with quark bubbles and then simply makes the replacement

$$n_f \to n_f - \frac{33}{2} \ , \tag{25}$$

i.e. one uses for b the full 1-loop QCD β-function coefficient $b = (33-2n_f)/12\pi$.

In fact the β-function in QCD (unlike QED) cannot be associated with vacuum polarization graphs alone, and there is no set of graphs that corresponds precisely to Eq. (23) with $b = (33 - 2n_f)/12\pi$. Nevertheless the naive non-Abelianization procedure seems to work quite well in predicting the high-order coefficients in perturbation theory. An impressive example is the weak-coupling expansion of the average plaquette in quenched ($n_f = 0$) lattice QCD.[31] For this quantity the perturbative coefficients c_n in Eq. (23) up to $n = 8$, suitably re-interpreted to allow for the difference between the lattice and continuum definitions of α_s, have been shown [31] to be dominated by a renormalon contribution of the form (24) with $b = 11/4\pi$ and $p = 2$.

Although the series (23) is divergent, it is not useless: it is expected to be an asymptotic expansion. By this we mean that the series truncated at order $n = m$ is an approximation to the true value of F, with an error bounded by

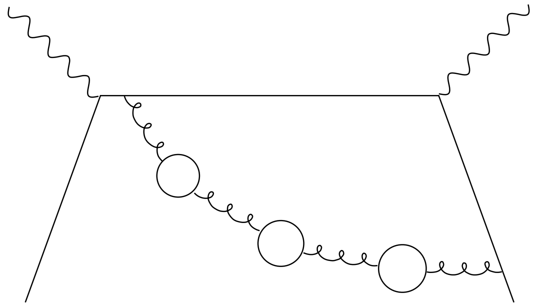

Figure 7: A graph containing a "renormalon chain".

the last term retained, $c_m \alpha_s^m$. Now the coefficients c_n satisfy

$$\frac{c_n}{c_{n-1}} \sim n \frac{b}{p} \tag{26}$$

and thus the smallest term occurs at $n = m \sim p/b\alpha_s$. Truncating the series at this point, we obtain the minimal ambiguity in the prediction of F, which is

$$\delta F \sim m!\, m^{-m} \sim e^{-m} \sim \exp\left(-\frac{p}{b\alpha_s}\right) . \tag{27}$$

Noting that

$$\alpha_s \sim \frac{1}{b \ln(Q^2/\Lambda^2)} \tag{28}$$

where Q^2 is the relevant hard scattering scale, we see that

$$\delta F \sim \left(\frac{\Lambda^2}{Q^2}\right)^p . \tag{29}$$

We may distinguish two cases:

1. $p < 0$. In QCD, this is an *ultraviolet* renormalon. The divergent series (23) has alternating signs. It might appear from Eq. (29) that this will lead to an ambiguity in F that grows with increasing Q^2. In fact, however, the series can be summed unambiguously in this case and there is no renormalon ambiguity.

2. $p > 0$, which is called an *infrared* renormalon. All the terms of the divergent series have the same sign and it cannot be summed unambiguously. The ambiguity (29) decreases like Q^{-2p} with increasing Q^2.

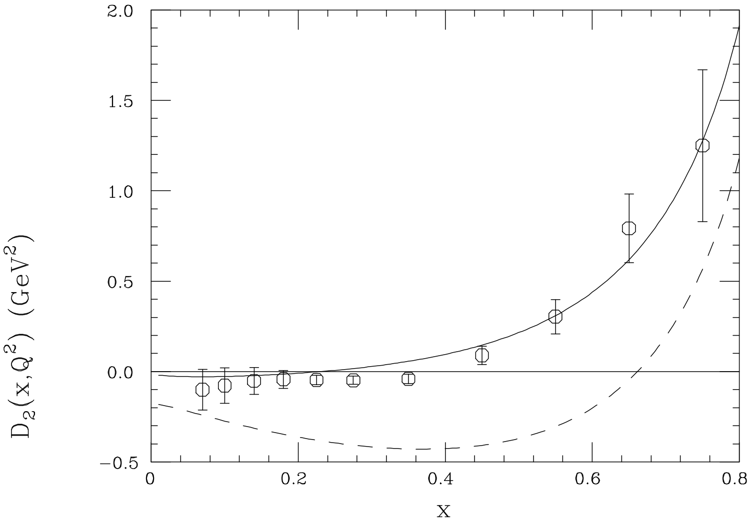

Figure 8: Power corrections to F_2 (solid) and xF_3 (dashed). Points are values deduced from BCDMS and SLAC data on F_2 (see text).

The above general discussion has some interesting possible applications to deep inelastic scattering. In the case of ultraviolet renormalons, various techniques can be used to sum the divergent terms and thus improve the precision of the perturbative prediction.[27−30] Infrared renormalons, on the other hand, imply that the perturbative prediction must be supplemented by additional non-perturbative information. In DIS, the power-suppressed nature of the ambiguity suggests that the extra information required concerns *higher-twist* contributions. In fact one can show[32] that similar renormalon graphs generate an ambiguity in the coefficient of the leading Q^{-2p} (twist $2p+2$) contribution, which cancels the power-suppressed ambiguity in the twist-2 prediction.

Thus the presence of an infrared renormalon signals the need for a higher-twist contribution and tells us what its power dependence on Q^2 must be. This suggests that we could go further and explore the possibility that the Bjorken-x dependence of the renormalon also indicates the x-dependence of the higher-twist contribution. Phenomenologically, this appears to be the case.[33−36] Fig. 8 shows, for example, predictions[35,36] based on this idea for the $1/Q^2$-suppressed corrections to the structure functions F_2 and xF_3, expressed in the form

$$F(x,Q^2) \simeq xq(x,Q^2)\left(1+\frac{D_2(x,Q^2)}{Q^2}\right) \tag{30}$$

where q is the appropriate combination of quark distributions. The form of the coefficient D_2 for F_2 is similar to that deduced [37] from BCDMS [38] and SLAC [39] data, shown by the points. Recent results [40] on higher twist in xF_3 also look similar in shape to the relevant curve (dashed). It would clearly be of interest to include the type of higher-twist contributions suggested by this approach in global fits to deep inelastic scattering data.

5 Jet Production

The important topic of jet production in DIS has also seen recent theoretical and phenomenological progress. There are new results from complete next-to-leading-order (NLO) calculations of jet rates, which will be useful for improving measurements of the strong coupling [41] and the gluon distribution.[42] In addition there are new calculations on testing BFKL dynamics at small x with forward jet production as a trigger.

5.1 Jet Cross Sections in Next-to-Leading Order

At present there are two programs in use to compute the two-jet (plus beam remnant) cross section in NLO using a JADE [43] type of jet definition: PROJET [44] and DISJET.[45] There is now a new program, MEPJET,[46] which can be used to compute jet cross sections using any infrared-safe definition. In addition there is the promise of a general-purpose program for the NLO calculation of any infrared-safe quantity in DIS.[47]

Table 1: Predicted two-jet inclusive cross sections in DIS at LO and NLO, for four jet definition schemes and (at NLO) three different recombination schemes.

Scheme	LO	NLO (E)	NLO ($E0$)	NLO (P)
W	1020 pb	2082 pb	1438 pb	1315 pb
JADE	1020 pb	1507 pb	1387 pb	1265 pb
k_T	1067 pb	1038 pb	1014 pb	944 pb
cone	1107 pb	1203 pb	1232 pb	1208 pb

Results [51] on the inclusive two-jet cross section using MEPJET with a variety of jet definitions, for a particular set of acceptance cuts at HERA, are summarized in Table 1. The jet-defining scheme that has been most widely used for NLO calculations is the so-called W-scheme,[48] in which two particles or jets are clustered if their invariant mass-squared s_{ij} is less than $y_{\rm cut} W^2$, where $y_{\rm cut}$ is the jet resolution ($y_{\rm cut} = 0.02$ here) and W is the hadronic c.m. energy. Experimentally, the JADE clustering variable $M_{ij}^2 \equiv 2E_iE_j(1-\cos\theta_{ij})$ has been used in place of s_{ij}. A suggested improvement is the $k_\perp$-scheme,[49] in which $k_{\perp,ij}^2 \equiv 2\min\{E_i^2, E_j^2\}(1-\cos\theta_{ij})$, evaluated in the Breit frame of reference, is compared with a resolution scale (40 GeV^2 here). Alternatively, one may use instead a cone type of jet definition, in which clustering occurs if $(\eta_i - \eta_j)^2 + (\phi_i - \phi_j)^2 < 1$, where η and ϕ are the pseudorapidity and azimuth in the HERA lab frame. In all these schemes the way of defining the combined momentum after clustering can also be varied, leading to the so-called E, $E0$ and P recombination schemes.[50]

It can be seen from Table 1 that in the W and JADE schemes there are large values of the K-factor ($K \equiv$ [NLO-LO]/LO) and strong recombination scheme dependences, which are reduced in the $k_\perp$ and cone schemes. One worrying point is that the MEPJET results do not agree with those of PROJET and DISJET for the W or JADE schemes.[51] This makes it very desirable to have another independent calculation of these quantities, which is said to be coming in the near future.[52]

5.2 Forward Jet Production

The rate of production of fast ($x_{\rm jet} \gg x$) forward jets in DIS at small x has been proposed as a good probe of BFKL dynamics.[53,54] The idea (Fig. 9) is that for jet transverse momenta $p_{T,\rm jet}^2 \sim Q^2$ there is little scope for ordinary DGLAP evolution, while the condition $x_{\rm jet} \gg x$ means that BFKL evolution in $\log x$ is enhanced.

In order to show that there is a BFKL enhancement in forward jet production at small x, one should establish that the usual NLO calculation with DGLAP evolution is not able to explain the data. This is difficult because NLO processes like boson-gluon fusion with an extra jet are dominant in the selected kinematic region.[51] Thus NLO corrections are large and not well under control.

The data of the H1 collaboration,[55] together with the results of a recent calculation based on BFKL dynamics,[56] are shown in Fig. 10 as a function of Bjorken x. The H1 selection criteria for forward jets are $x_{\rm jet} > 0.025$, $0.5 < p_{T,\rm jet}^2/Q^2 < 4$, $p_{T,\rm jet} > 5$ GeV and $6° < \theta_{\rm jet} < 20°$, where $\theta_{\rm jet}$ is

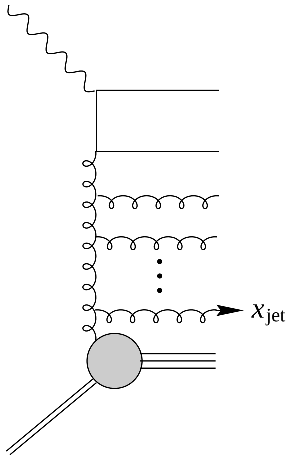

Figure 9: Forward jet production as a probe of BFKL dynamics.

the angle between the forward jet (defined by the cone algorithm) and the proton beam. The agreement between the BFKL calculation and the data is encouraging. The approximate matrix element calculation shown, performed by omitting the BFKL ladder in Fig. 9, falls well below the data. It will be important to check that this remains true when the full NLO matrix elements are included. For this purpose the new NLO programs discussed above, which allow the cone jet definition to be used, will be most valuable.

Acknowledgments

I am grateful to many colleagues, especially Yu.L. Dokshitzer, G. Marchesini, A.H. Mueller and G. Salam, for helpful discussions on the topics of this talk. It is also a pleasure to thank the organizers of DIS96 for arranging a most stimulating meeting in such a wonderful location. This work was supported in part by the U.K. Particle Physics and Astronomy Research Council and by the E.C. Programme “Human Capital and Mobility”, Network “Physics at High Energy Colliders”, contract CHRX-CT93-0357 (DG 12 COMA).

References

1. D.A. Harris, CCFR-NuTeV Collaboration, FERMILAB-CONF-95-144, to appear in *Proc. 30th Rencontres de Moriond, Meribel les Allues,*

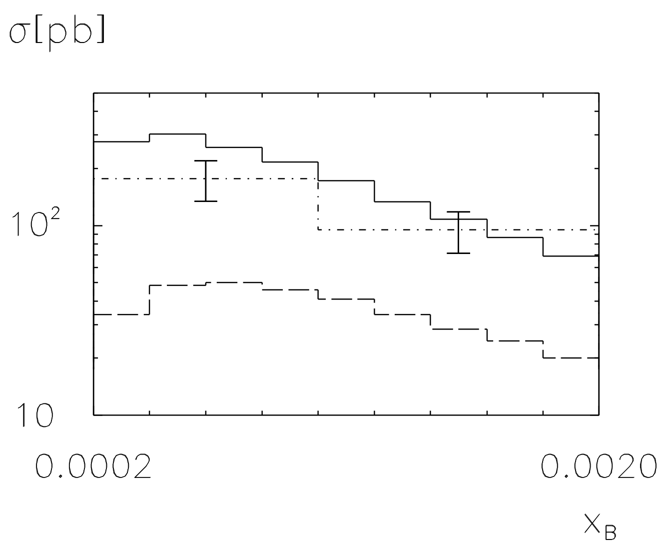

Figure 10: Forward jet production: BFKL calculation (solid), approximate three-parton matrix elements (dashed), and data of the H1 experiment (dot-dashed).

France, March 1995.

2. J. Ellis, E. Gardi, M. Karliner and M.A. Samuel, *Phys. Lett.* B **366**, 268 (1996).
3. V.N. Gribov and L.N. Lipatov, *Sov. J. Nucl. Phys.* **15**, 78 (1972);
   G. Altarelli and G. Parisi, *Nucl. Phys.* B **126**, 298 (1977);
   Yu.L. Dokshitzer, *Sov. Phys. JETP* **46**, 641 (1977).
4. Y.Y. Balitskiĭ and L.N. Lipatov, *Sov. Phys. JETP* **28**, 822 (1978);
   E.A. Kuraev, L.N. Lipatov, and V.S. Fadin, *ibid.* **45**, 199 (1977);
   L.N. Lipatov, *ibid.* **63**, 904 (1986).
5. V.S. Fadin and L.N. Lipatov, preprint DESY 96-020 [hep-ph/9602287].
6. R. Kirschner and L.N. Lipatov, *Nucl. Phys.* B **213**, 122 (1983).
7. B.I. Ermolaev, S.I. Manayenkov and M.G. Ryskin, preprint DESY 95-017 [hep-ph/9502262].
8. R.L. Heimann, *Nucl. Phys.* B **64**, 429 (1973).
9. J. Bartels, B.I. Ermolaev and M.G. Ryskin, *Z. Phys.* C **70**, 273 (1996).
10. J. Blümlein and A. Vogt, *Phys. Lett.* B **370**, 149 (1996).
11. J. Bartels, B.I. Ermolaev and M.G. Ryskin, preprint DESY 96-025 [hep-ph/9603204].
12. L.V. Gribov, E.M. Levin, and M.G. Ryskin, *Phys. Rep.* **100**, 1 (1983).

13. A.H. Mueller, *Nucl. Phys.* B **415**, 373 (1994); *ibid.* **437**, 107 (1995).
14. A.H. Mueller and B. Patel, *Nucl. Phys.* B **425**, 471 (1994).
15. Z. Chen and A.H. Mueller,*Nucl. Phys.* B **451**, 579 (1995).
16. G.P. Salam, *Nucl. Phys.* B **449**, 589 (1995); *ibid.* **461**, 512 (1996).
17. A.H. Mueller and G.P. Salam, preprint CU-TP-746 [hep-ph/9605302].
18. N.N. Nikolaev, B.G. Zakharov, and V.R. Zoller, *JETP Lett.* **59**, 6 (1994).
19. B. Andersson, G. Gustafson and J. Samuelsson, *Nucl. Phys.* B **467**, 443 (1996).
20. H. Navelet, R. Peschanski and C. Royon, *Phys. Lett.* B **366**, 329 (1996); H. Navelet, R. Peschanski, C. Royon and S. Wallon, preprint SACLAY-SPHT-96-043 [hep-ph/9605389].
21. G.P. Salam, preprint Cavendish-HEP 95/07 [hep-ph/9601220].
22. G.P. Salam, these Proceedings.
23. For reviews and classic references see V.I. Zakharov, *Nucl. Phys.* B **385**, 452 (1992) and A.H. Mueller, in *QCD 20 Years Later*, vol. 1 (World Scientific, Singapore, 1993).
24. M. Beneke, *Nucl. Phys.* B **405**, 424 (1993);
M. Beneke and V.M. Braun, *Nucl. Phys.* B **426**, 301 (1994).
25. D.J. Broadhurst, *Z. Phys.* C **58**, 339 (1993);
J.A. Gracey, *Phys. Lett.* B **323**, 141 (1994).
26. D.J. Broadhurst and A.L. Kataev, *Phys. Lett.* B **315**, 179 (1993).
27. C.N. Lovett-Turner and C.J. Maxwell, *Nucl. Phys.* B **452**, 188 (1995).
28. D.J. Broadhurst and A.G. Grozin, *Phys. Rev.* D **52**, 4082 (1995);
M. Neubert, *Phys. Rev.* D **51**, 5924 (1995).
29. M. Beneke and V.M. Braun, *Phys. Lett.* B **348**, 513 (1995).
30. P. Ball, M. Beneke and V.M. Braun, *Nucl. Phys.* B **452**, 563 (1995).
31. F. Di Renzo, E. Onofri and G. Marchesini, *Nucl. Phys.* B **457**, 202 (1995).
32. A.H. Mueller, *Phys. Lett.* B **308**, 355 (1993).
33. V.M. Braun, to appear in *Proc. 30th Rencontres de Moriond, Meribel les Allues, France, March 1995* [hep-ph/9505317].
34. E. Stein, M. Meyer-Hermann, L. Mankiewicz and A. Schäfer, *Phys. Lett.* B **376**, 177 (1996); M. Meyer-Hermann, M. Maul, L. Mankiewicz, E. Stein and A. Schäfer, preprint UFTP-414-1996 [hep-ph/9605229].
35. Yu.L. Dokshitzer, G. Marchesini and B.R. Webber, preprint CERN-TH/95-281 [hep-ph/9512336], to be published in *Nucl. Phys.* B.
36. M. Dasgupta and B.R. Webber, preprint Cavendish-HEP-96-1 [hep-ph/9604388], to be published in *Phys. Lett.* B.
37. M. Virchaux and A. Milsztajn, *Phys. Lett.* B **274**, 221 (1992).

38. BCDMS Collaboration, A.C. Benvenuti et al., *Phys. Lett.* B **223**, 485 (1989); *ibid.* **237**, 592 (1990).
39. L.W. Whitlow et al., *Phys. Lett.* B **282**, 475 (1992).
40. A.V. Sidorov, preprint JINR-E2-96-254 [hep-ph/9607275].
41. H1 Collaboration, T. Ahmed et al., *Phys. Lett.* B **346**, 415 (1995); ZEUS Collaboration, M. Derrick et al., *Phys. Lett.* B **363**, 201 (1995).
42. H1 Collaboration, T. Ahmed et al., *Nucl. Phys.* B **449**, 3 (1995).
43. JADE Collaboration, W. Bartel et al., *Z. Phys.* C **33**, 23 (1986).
44. D. Graudenz, *Phys. Rev.* D **49**, 3291 (1994); *Comp. Phys. Commun.* **92**, 65 (1995).
45. T. Brodkorb and E. Mirkes, preprint MAD/PH/821 [hep-ph/9404287]; *Z. Phys.* C **66**, 141 (1995).
46. E. Mirkes and D. Zeppenfeld, preprint TTP95-42 [hep-ph/9511448].
47. S. Catani and M.H. Seymour, preprint CERN-TH/96-28 [hep-ph/9602277], to be published in *Phys. Lett.* B; preprint CERN-TH/96-29 [hep-ph/9605323].
48. J.G. Körner, E. Mirkes and G. Schuler, *Int. J. Mod. Phys.* A **4**, 1781 (1989); T. Brodkorb, J.G. Körner, E. Mirkes, and G. Schuler, *Z. Phys.* C **44**, 415 (1989).
49. S. Catani, Yu.L. Dokshitzer and B.R. Webber, *Phys. Lett.* B **285**, 291 (1992).
50. See, for example, S. Bethke, Z. Kunszt, D.E. Soper and W.J. Stirling, *Nucl. Phys.* B **370**, 310 (1992).
51. E. Mirkes and D. Zeppenfeld, preprint TTP96-10 [hep-ph/9604281].
52. S. Catani and M.H. Seymour, private communication.
53. A.H. Mueller,*Nucl. Phys.* B (Proc. Suppl.) **18C**, 125 (1990); *J. Phys.* G **17**, 1443 (1991).
54. J. Kwiecinski, A.D. Martin and P.J. Sutton, *Phys. Rev.* D **46**, 921 (1992);
J. Bartels, A. De Roeck and M. Loewe, *Z. Phys.* C **54**, 635 (1992);
W.-K. Tang, *Phys. Lett.* B **278**, 363 (1992).
55. H1 Collaboration, S. Aid et al., *Phys. Lett.* B **356**, 118 (1995).
56. J. Bartels, V. Del Duca, A. De Roeck, D. Graudenz and M. Wüsthoff, preprint DESY 96-036 [hep-ph/9604272].